







Article

Analysis of MONARC and ACTIVATE Airborne Aerosol Data for Aerosol-Cloud Interaction Investigations: Efficacy of Stairstepping Flight Legs for Airborne In Situ Sampling

Hossein Dadashazar^{1,*}, Ewan Crosbie^{2,3}, Yonghoon Choi^{2,3}, Andrea F. Corral¹, Joshua P. DiGangi², Glenn S. Diskin², Sanja Dmitrovic⁴, Simon Kirschler^{5,6}, Kayla McCauley⁷, Richard H. Moore², John B. Nowak², Claire E. Robinson^{2,3}, Joseph Schlosser¹, Michael Shook², Kenneth Lee Thornhill², Christiane Voigt^{5,6}, Edward L. Winstead^{2,3}, Luke D. Ziemba² and Armin Sorooshian^{1,4,7,*}

¹ Department of Chemical and Environmental Engineering, University of Arizona, Tucson, AZ 85721, USA

² NASA Langley Research Center, Hampton, VA 23666, USA

³ Science Systems and Applications, Inc., Hampton, VA 23666, USA

⁴ James C. Wyant College of Optical Sciences, University of Arizona, Tucson, AZ 85721, USA

⁵ Institute of Atmospheric Physics, German Aerospace Center, 53227 Bonn, Germany

⁶ Institute of Atmospheric Physics, University Mainz, 55122 Mainz, Germany

⁷ Department of Hydrology and Atmospheric Sciences, University of Arizona, Tucson, AZ 85721, USA

* Correspondence: hosseind@arizona.edu (H.D.); armin@arizona.edu (A.S.)



Citation: Dadashazar, H.; Crosbie, E.; Choi, Y.; Corral, A.F.; DiGangi, J.P.; Diskin, G.S.; Dmitrovic, S.; Kirschler, S.; McCauley, K.; Moore, R.H.; et al. Analysis of MONARC and ACTIVATE Airborne Aerosol Data for Aerosol-Cloud Interaction Investigations: Efficacy of Stairstepping Flight Legs for Airborne In Situ Sampling. *Atmosphere* **2022**, *13*, 1242. <https://doi.org/10.3390/atmos13081242>

Academic Editor: Suzanne Crumeyrolle

Received: 10 July 2022

Accepted: 2 August 2022

Published: 5 August 2022

Publisher's Note: MDPI stays neutral with regard to jurisdictional claims in published maps and institutional affiliations.



Copyright: © 2022 by the authors. Licensee MDPI, Basel, Switzerland. This article is an open access article distributed under the terms and conditions of the Creative Commons Attribution (CC BY) license (<https://creativecommons.org/licenses/by/4.0/>).

Abstract: A challenging aspect of conducting airborne in situ observations of the atmosphere is how to optimize flight plans for specific objectives and constraints associated with weather and flight restrictions. For aerosol-cloud interaction research, two recent campaigns utilized a “stairstepping” approach whereby an aircraft conducts level legs at various altitudes while moving forward with each subsequent leg: the 2019 MONterey Aerosol Research Campaign (MONARC) over the north-east Pacific and the 2020–2022 Aerosol Cloud meTeorology Interactions oVer the western ATLantic Experiment (ACTIVATE) over the northwest Atlantic. We examine the homogeneity of several atmospheric variables both vertically and horizontally in the marine boundary layer with a focus on the sub-cloud environment. In well-mixed boundary layers, there was generally good horizontal and vertical homogeneity in potential temperature, winds, water vapor mixing ratio, various trace gases, and many aerosol variables. Selected aerosol variables exhibited the most variability owing to sensitivity to humidity and near-cloud conditions (supermicrometer aerosol concentrations), coastal pollution gradients (e.g., organic aerosol mass), and small spatial scale phenomena such as new particle formation (aerosol number concentration for particles with diameter >3 nm). Illustrative cases are described when stairstepping can pose issues requiring extra caution for data analysis: (i) poor vertical mixing and layers decoupled from those below; (ii) multiple cloud layers; (iii) fluctuating cloud base/top and boundary layer top heights; and (iv) horizontal variability across specific features leading to sharp gradients such as right near coastlines and over the Gulf Stream with strong sea surface temperature changes. Results from this study provide a guide both for future studies aiming to examine these mission datasets and for designing new airborne campaigns.

Keywords: ACTIVATE; airborne sampling; aerosol; cloud; in situ observations

1. Introduction

A challenge in airborne flight science targeting marine boundary layer (MBL) processes is how to optimize flight plans to characterize the horizontal and vertical dimensions with high spatial resolution (~hundreds of meters). How best to fly in the MBL depends largely on research goals, instrument payload requirements, and flight constraints. For instance, research into surface fluxes (as measured by co-variance) benefit from flying the lowest possible leg within a surface mixed layer [1]. Studies on cloud top entrainment

warrant slant patterns near cloud top in a sawtooth pattern [2]. Of interest to the current study is investigation into aerosol-cloud interactions, for which certain vertical layers are of interest including: (i) as low as possible over the sea surface to characterize surface fluxes; (ii) immediately below cloud base to characterize terms relevant for understanding aerosol-cloud interactions (e.g., updraft velocity and/or vertical wind statistics, aerosol size distribution, aerosol composition); (iii) legs in cloud, often above base and below top, to characterize cloud microphysical properties, entrainment, and cloud processing; and (iv) at least one leg above cloud to sample the overlying environment.

A common flight strategy to conduct horizontal and vertical characterization of atmospheric variables relevant to aerosol-cloud interactions is to fly stacked level legs (“wall” pattern) [3]. These patterns have the downside of being limited in horizontal coverage as a typical 5–10 min leg in a wall covers only few tens of kilometers depending on aircraft airspeed. Horizontal coverage is desirable as variability in weather and pollution characteristics helps populate data across a wider dynamic range of values for variables relevant to aerosol-cloud interactions. Sawtooth [2] and “spiral” (i.e., ascending or descending in a circular shape) soundings [4] are limited in terms of statistics at a fixed level, which is critical for some data types (e.g., winds, aerosol size distributions, and composition) requiring tens of seconds of time for robust calculation of desired quantities. Another strategy is “stairstepping”, which incorporates enough time at a level altitude for building sufficient statistics for the most time-demanding measurements, while allowing for probing different vertical levels across a wider horizontal range as compared to a wall or soundings; the limitation is that the level legs are not on top of each other to provide a detailed characterization of a vertical atmospheric column. Numerous campaigns have utilized some version of a stairstepping approach including the Cloud System Evolution in the Trades (CSET) [5], the Southern Ocean Clouds, Radiation, Aerosol Transport Experimental Study (SOCRATES) [6], and the Holistic Interactions of Shallow Clouds, Aerosols and Land Ecosystems (HI-SCALE) campaign [7], all three of which studied aerosol and cloud properties. While this strategy of flying is not new, there have been limited attempts to quantitatively characterize how well the strategy works and, more broadly, how success can even be assessed.

Two recent airborne experiments targeting aerosol-cloud interactions used stairstepping to produce datasets that afford the opportunity to explore how well the flight strategy works in terms of horizontal and vertical characterization. These experiments include the MONterey Aerosol Research Campaign (MONARC) and the Aerosol Cloud meTeorology Interactions oVer the western ATLantic Experiment (ACTIVATE). A challenge is how best to quantify the success of such a strategy and this work aims to do this quantitatively in a few ways. Some variables are expected to change more spatially such as aerosol properties owing to spatial and temporal patterns in emissions, growth processes, transformations, and sinks, in addition to sensitivity to ambient meteorology. Section 2 of this work summarizes the data and methods, while Section 3 presents the following analyses: (i) comparing atmospheric variable values both vertically and horizontally in the MBL separately for two regions where these campaigns took place (northeast Pacific and northwest Atlantic) (Sections 3.1 and 3.2); (ii) quantifying various measures of variability horizontally for individual leg types (Section 3.2); and (iii) discussion of case study situations requiring extra attention and guidance about how to adapt to such scenarios (Section 4). Section 5 concludes with a discussion and conclusions. Implications of this work range from providing guidance for the interpretation of surface-based ocean measurements (e.g., ships and buoys) used as a proxy for sub-cloud conditions to aiding decisions about flight paths for future in situ airborne measurements. These results provide a useful resource for the interpretation of MONARC and ACTIVATE datasets, with implications still for past and future airborne in situ campaigns using stairstepping.

2. Methods

2.1. Field Campaigns and Flight Approach

The MONterey Aerosol Research Campaign (MONARC) involved 14 research flights based out of Marina, California between May and June 2019 with the Center for Remotely-Piloted Aircraft Studies (CIRPAS) Twin Otter [8]. The goal of this mission was to characterize aerosol-cloud interactions over the northeast Pacific using out-and-back flights (~5 h) over the same path each day (Figure 1a). The Aerosol Cloud meTeorology Interactions oVer the western ATLantic Experiment (ACTIVATE) involved 40 research flights in its first year of flights between 14 February–12 March 2020 and 13 August–30 September 2020 [9]. The out-and-back flights (~3–4 h) comprised two aircraft in vertical coordination deployed from NASA Langley Research Center in Hampton, Virginia to sample the northwest Atlantic (Figure 1b). The low-flying aircraft, the HU-25 Falcon, conducted in situ measurements of trace gases, aerosol particles, clouds, and meteorological variables in the MBL (≤ 3 km). Although not relevant to this work, the high-flying (~9 km) King Air deployed remote sensors and launched dropsondes.

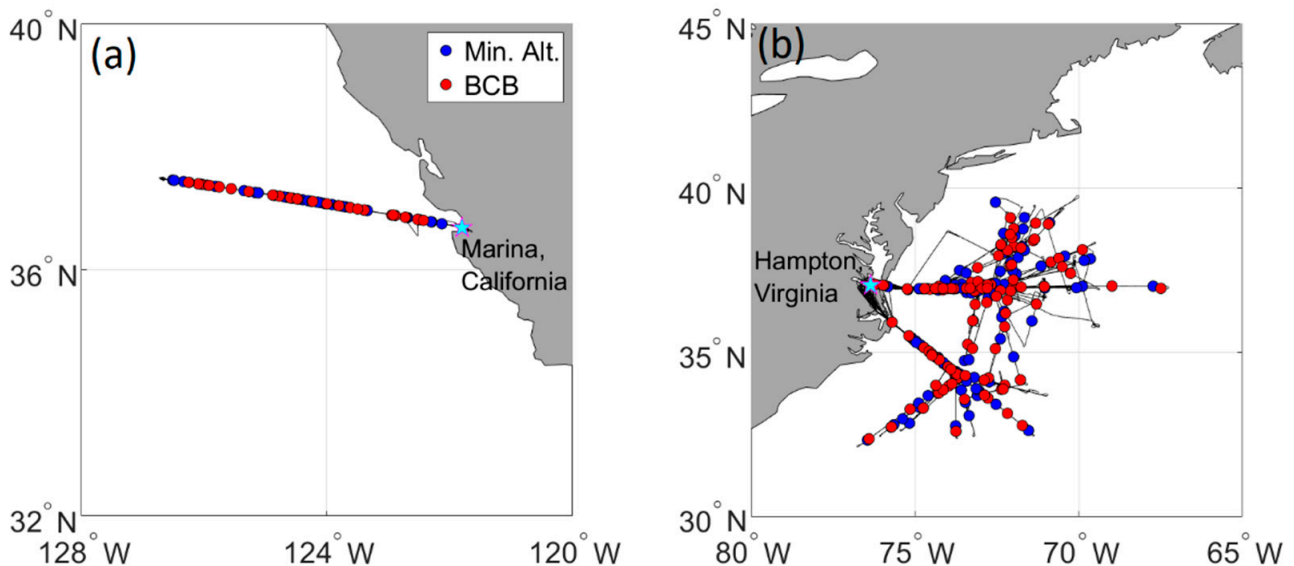


Figure 1. The midpoints of Minimum Altitude (Min. Alt.) and below cloud base (BCB) legs, described more below, overlaid on flight tracks conducted in (a) MONARC (May 2019–June 2019) and (b) ACTIVATE (February 2020–March 2020 and August 2020–September 2020).

The flight approach for both campaigns was similar (Figure 2) and thus we describe first specifically how ACTIVATE was designed, followed by MONARC which only varied slightly. Flights were flown in repeated stairstepping “ensembles” to be both (i) adaptable to variable cloud conditions and boundary layer structure and (ii) prescriptive, such that a set of governing rules made implementation and decision making less subjective.

During ACTIVATE, the Falcon flew at ~ 120 m s^{-1} and conducted level legs at key altitudes for a duration of ~ 3 min (~ 20 – 25 km). The standard “cloud” ensemble comprised two pairs of level legs flown adjacent to the cloud base; alternating between ~ 100 m below the estimated cloud base and ~ 100 m above the estimated cloud base (BCB = below cloud base and ACB = above cloud base, respectively). Upon completion, the aircraft descended to the minimum operational altitude (Min. Alt.: ~ 150 m Above Sea Level (ASL)) for a level leg before climbing to approximately ~ 150 m above the estimated cloud top altitude (ACT = above cloud top) for a level leg, providing a continuous profile across all altitudes of interest. The last leg of the ensemble was approximately ~ 100 m below the cloud tops (BCT = below cloud top). Typical cloud ensembles lasted 35 min spanning ~ 250 km. The standard “clear” ensemble mimicked the last three legs of the “cloud” module except that the cloud top estimate was replaced with an estimate of the top of the MBL or, in some

cases, the residual continental boundary layer, providing sampling at Min. Alt., above the boundary layer top (ABL), and below the boundary layer top (BBL).

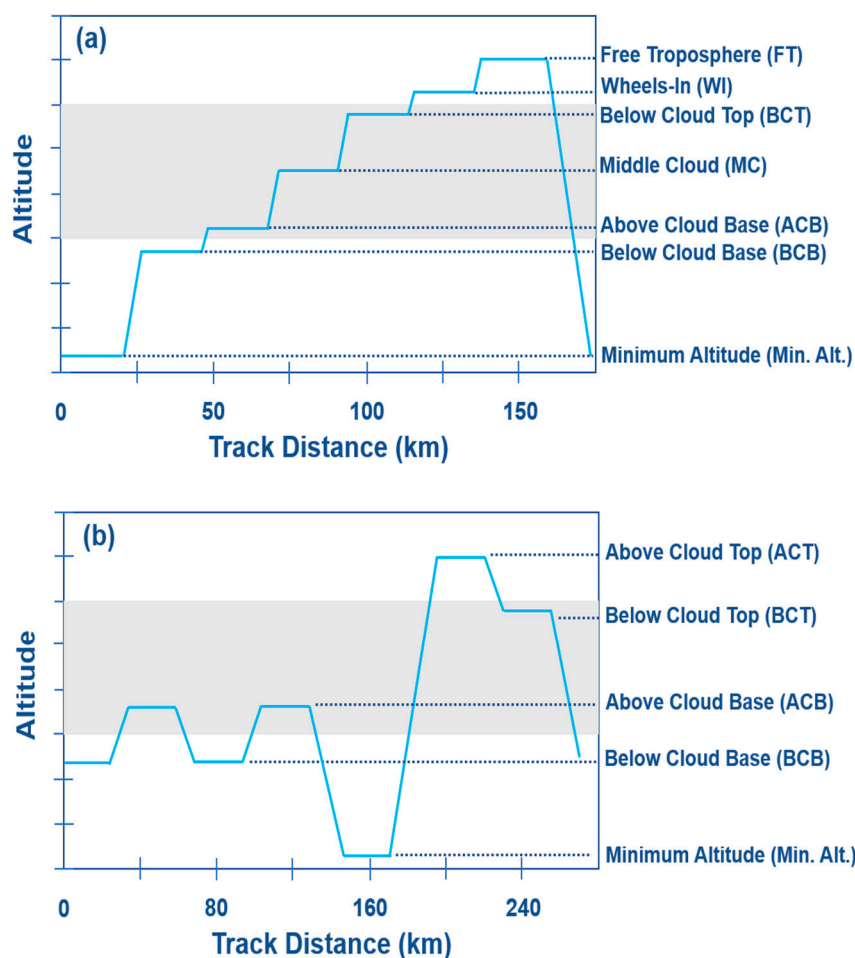


Figure 2. Typical flight path conducted during cloud ensembles of (a) MONARC 2019 and (b) 2020 ACTIVATE research flights, with gray shading representing a cloud layer. Clear ensembles including a Min. Alt. leg followed by below boundary layer top (BBL) and above boundary layer top (ABL) legs and then a slant descent back to Min. Alt.

Ascending and descending transitions were designed to allow a revised estimate of cloud base, cloud top, or MBL height, either visually or through real-time data. Leg altitudes were then adjusted accordingly and if the boundary was less well defined, the offset altitude differentials were increased (e.g., to stay below cloud on a BCB leg). Sometimes cloud tops were so variable as to preclude providing any reasonable estimate (e.g., in summertime conditions where convective development was prevalent), and occasionally multiple cloud layers interacted in a complex environment. These unorthodox cases required some additional judgement and were flown on a more ad hoc basis. In a few special cases, bonus legs were added to capture features such as aerosol layers in the free troposphere. During clear air sampling with high aircraft coincidence, a remote sensing leg (RS) was sometimes added between BBL and Min. Alt. (at a fixed altitude of 250 m) to aid lidar and in situ aerosol comparisons near the surface, although those are not focused on in this work.

MONARC cloud ensembles had slight differences as compared to those in ACTIVATE to leverage the clouds more typical of the northeast Pacific having well-defined vertical extent and a strong capping inversion. The legs were as follows in order: minimum altitude (Min. Alt.) leg below ~60 m ASL, below cloud base (BCB), above cloud base (ACB), mid-cloud (MC), below cloud top (BCT), wheels-in (WI; right above top with wheels ideally

positioned at cloud top), above cloud top (ACT), descent back down to Min. Alt. to start a new ensemble. The wheels-in leg was more suitable in MONARC (versus ACTIVATE) owing to the more well-defined cloud tops. Standard clear ensembles were identical to ACTIVATE with the caveat that sometimes multiple BBL legs were completed at different altitudes to obtain more vertically-resolved information. At the farthest west point of each MONARC flight, a spiral sounding was conducted. The Twin Otter typically flew at $\sim 55 \text{ m s}^{-1}$, with the duration of each leg and ensemble being 6 min ($\sim 20 \text{ km}$) and 50 min ($\sim 165 \text{ km}$), respectively.

2.2. Data Variables and Measurements

The relevant instrument data used from ACTIVATE (HU-25 only) and MONARC are summarized in Table 1, including diameter ranges (if relevant) and the instrument name and manufacturer. This work relies on only a subset of all the measurements deemed sufficient to achieve objectives of this study. Beginning with ACTIVATE which had a larger payload, aerosol number concentrations (N_a) were recorded for different diameter ranges using a combination of two condensation particle counters (CPCs; $>3 \text{ nm}$ and $>10 \text{ nm}$), a laser aerosol spectrometer (LAS; $0.1\text{--}5 \text{ }\mu\text{m}$), and a fast cloud droplet probe (FCDP; $3\text{--}50 \text{ }\mu\text{m}$). Submicrometer aerosol composition for non-refractory species was measured with an Aerodyne Aerosol Mass Spectrometer (AMS), with only sulfate and organics used here as they were the most abundant components. Cloud data included cloud drop number concentrations (N_d ; $3\text{--}50 \text{ }\mu\text{m}$), liquid water content (LWC: $3\text{--}50 \text{ }\mu\text{m}$) from the FCDP, and rainwater content (RWC: $51.3\text{--}1464.9 \text{ }\mu\text{m}$) from a two-dimensional optical array imaging probe (2DS; SPEC Inc., Kansas City, KS, USA) [10,11]. Trace gas concentrations were measured with a combination of a PICARRO G2401 gas concentration analyzer (CH_4 , CO_2 , CO), a 2B Technologies dual beam photometer (O_3), and a diode laser hygrometer (DLH; H_2O). Various meteorologically-relevant variables such as wind speed and temperature were measured from the Turbulent Air Motion Measurement System (TAMMS) and a Rosemount 102 total temperature sensor, respectively. All ACTIVATE variables were measured at 1 s time resolution except for most gases (CH_4 , CO_2 , CO , O_3 , 0.5 Hz), winds (20 Hz), and the AMS that operated in 1 Hz Fast-MS mode with data averaged to 25 s time resolution [12]. As shown in Table 1, measured variables in MONARC (all 1 s resolution) were similar to those from ACTIVATE with the use of different instruments and model numbers.

Table 1. List of relevant variables for this study as measured by the Twin Otter in 2019 MONARC (M) flights and from the Falcon in 2020 ACTIVATE (A) flights, including instrument information.

Mission	Variable	Diameter	Instrument	Manufacturer/Reference
A/M	Aerosol number concentration ($N_{a>3\text{nm}}$)	$>3 \text{ nm}$	Condensation Particle Counter (CPC), model 3776 (A) and 3025 (M)	TSI Inc.; [13]
A/M	Aerosol number concentration ($N_{a>10\text{nm}}$)	$>10 \text{ nm}$	Condensation Particle Counter (CPC), model 3772 (A) and 3010 (M)	TSI Inc.; [13]
A	Aerosol number concentration ($N_{a100\text{--}1000\text{nm}}$)	$100\text{--}1000 \text{ nm}$	Laser Aerosol Spectrometer (LAS), model 3340	TSI Inc.; [14]
A	Aerosol number concentration ($N_{a>1000\text{nm}}$)	$1\text{--}5 \text{ }\mu\text{m}$	Laser Aerosol Spectrometer (LAS), model 3340	TSI Inc.; [14]
A	Aerosol number concentration ($N_{a>3000\text{nm}}$)	$3\text{--}50 \text{ }\mu\text{m}$	Fast Cloud Droplet Probe (FCDP)	SPEC Inc.; [15]
M	Aerosol number concentration ($N_{a127\text{--}901\text{nm}}$)	$127\text{--}901 \text{ nm}$	Passive Cavity Aerosol Spectrometer Probe (PCASP)	PMS Inc., modified by DMT Inc.; [16]

Table 1. Cont.

Mission	Variable	Diameter	Instrument	Manufacturer/Reference
M	Aerosol number concentration ($N_{a>901nm}$)	901–3390 nm	Passive Cavity Aerosol Spectrometer Probe (PCASP)	PMS Inc., modified by DMT Inc.; [16]
M	Aerosol number concentration ($N_{a>3270nm}$)	3.27–36 μm	Forward Scattering Spectrometer Probe (FSSP)	PMS Inc., modified by DMT Inc.; [16]
A	Organic, sulfate mass concentration	<1 μm	High-Resolution Time-of-Flight Aerosol Mass Spectrometer (AMS)	Aerodyne; [17]
A	Liquid water content	3–50 μm	Fast Cloud Droplet Probe	SPEC Inc.; [15]
M	Liquid water content	3–50 μm	Particle Volume Monitor-100A	[18]
A	Rain water content	51.3–1464.9 μm	2DS Stereo Probe	SPEC Inc.; [11]
M	Rain water content	16–1563 μm	Cloud Imaging Probe	Droplet Measurement Technologies, Inc.
A	Methane concentration (CH_4)	–	G2401 gas concentration analyzer	PICARRO; [19]
A	Carbon dioxide concentration (CO_2)	–	G2401 gas concentration analyzer	PICARRO; [19]
A	Carbon monoxide concentration (CO)	–	G2401 gas concentration analyzer	PICARRO; [19]
A	Ozone concentration (O_3)	–	Dual Beam Photometer, Model 205	PICARRO; [19]
A	Water vapor (H_2O)	–	Diode Laser Hygrometer (DLH)	[20]
M	Water vapor (H_2O)	–	Chilled Mirror Hygrometer	EdgeTech Vigilant; [16]
A	Horizontal wind speed (Wind)	–	Turbulent Air-Motion Measurement System (TAMMS)	[21]
M	Horizontal wind speed (Wind)	–	Five-Hole Radome Gust Probe	[16]

2.3. Calculations

For calculations of data variables along level aircraft legs presented in this study, extra details are described here:

- Aerosol variables (i.e., measurements provided by CPCs, LAS, PCASP) were screened to remove possible contamination due to the presence of cloud or rain. A strict approach was taken to omit aerosol data in a window of 2 s before and after when either liquid water content or rain water content exceeded 0.005 g m^{-3} .
- In the case of more than one leg (typically 2) flown at the same vertical level in a single ensemble (e.g., two BCB legs in cloud ensembles of ACTIVATE), the one that was closer in distance to the Min. Alt. leg was selected for analyses requiring a comparison of adjacent Min. Alt. and BCB leg data.
- The distance between two legs was calculated based on the distance between the midpoints of the two legs using the great circle equation [22].
- As part of our analysis centers around how well measured values of common variables agree between different legs, statistical analysis was performed. First, linear regressions were performed to assess the degree of correlation between measured variables in two legs. Second, similarity between leg-mean values of specific variables (x_i) between two legs was quantified using the mean absolute relative deviation (MARD):

$$\text{MARD} = \frac{2}{n} \sum_{i=1}^n \frac{|x_{i, \text{leg1}} - x_{i, \text{leg2}}|}{|x_{i, \text{leg1}} + x_{i, \text{leg2}}|} \quad (1)$$

where n is the total number of leg pairs examined. MARD is unitless as its normalized by the averages of two legs. For variable values greater than zero, MARD is between 0 and 2 with values closer to 0 associated with more similarity between two legs.

- The standard deviation in horizontal wind speed (σ_{wind}) was calculated as a measure of turbulence in the MBL. Higher σ_{wind} values indicate more turbulence and likely greater vertical mixing in the MBL. Furthermore, potential temperature (θ) was derived using measurements from Table 1.

3. Results

3.1. Vertical Comparisons

We begin by comparing data values between adjacent Min. Alt. and either BCB or BBL legs since they are adjacent legs in horizontal space within a single cloud or clear ensemble, respectively. It is presumed that data from each pair of legs should yield similar values in a well-mixed MBL for variables without small spatial scale gradients. The results agree with this notion, although there are some exceptions as discussed below. A factor contributing to differences in measurement values between legs being compared is wind direction relative to aircraft heading. Horizontal homogeneity should increase when sampling along the wind in contrast to crosswind situations. As in any field campaign there will be imperfect alignment between an aircraft and wind direction at certain times. As a result, we examine the datasets without any special consideration of wind direction to keep the results more generalizable.

3.1.1. MONARC

Table 2 summarizes MONARC’s descriptive statistics for data variables between Min. Alt. and the associated BCB or BBL leg for each cloud or clear ensemble, respectively. The median flight altitude of Min. Alt. legs was 32 m for both cloud and clear ensembles, respectively, in contrast to 218/190 m for both BCB/BBL legs. The average horizontal distance between Min. Alt. and BCB/BBL legs was 22/21 km.

Table 2. Statistics for selected aerosol, gaseous, and meteorological variables measured during MONARC 2019 flights. Statistics are calculated for Min. Alt./BCB legs and Min. Alt./BBL legs for cloud and clear ensembles, respectively, in the first two data columns (additional statistics for 25th/75th percentiles and minimum/maximum values are in Table S1). The rightmost three columns report correlation statistics between different leg pairs conducted at different heights within the MBL for cloud (i.e., Min. Alt. and BCB) and clear (i.e., Min. Alt. and BBL) ensembles during MONARC 2019 flights.

Parameter	(Min. Alt./BCB)/(Min. Alt./BBL)		Cloud/Clear		
	Median	No. Pairs	Slope	R ²	MARD
Altitude (m)	(32/218)/(32/190)	31/30	-	-	-
N _{a>3nm} (cm ⁻³)	(329/349)/(1041/1035)	23/26	0.59/0.95	0.68/0.84	0.24/0.18
N _{a>10nm} (cm ⁻³)	(281/292)/(728/802)	23/26	0.64/0.77	0.69/0.73	0.25/0.24
N _{a127-901nm} (cm ⁻³)	(51/47)/(138/125)	23/26	0.93/0.86	0.97/0.83	0.26/0.15
N _{a>901nm} (cm ⁻³)	(0.97/0.75)/(2.29/1.85)	23/26	0.63/0.92	0.75/0.66	0.44/0.35
N _{a>3270nm} (cm ⁻³)	(0.92/1.83)/(0.82/0.76)	23/26	2.83/1.87	0.43/0.46	0.75/0.50
H ₂ O (g kg ⁻¹)	(8.4/8.3)/(7.9/7.2)	31/30	1.18/0.51	0.94/0.12	0.03/0.14
wind (m s ⁻¹)	(11.3/13.0)/(11.8/14.2)	31/30	1.09/1.21	0.94/0.84	0.10/0.23
σ_{wind} (m s ⁻¹)	(0.5/0.4)/(0.6/0.5)	31/30	0.57/0.77	0.34/0.77	0.27/0.32
θ (K)	(284.9/284.9)/(285.2/285.3)	31/30	1.18/1.44	0.80/0.93	0.00/0.00

There was generally good agreement for thermodynamic and meteorological variables consistent with coupling and mixing between the different levels. The agreement in potential temperature was especially strong between Min. Alt.-BCB and Min. Alt.-BBL leg pairs, with the ratio of the leg-median value between the two pairs of legs similarly being 1.0. Ratios between the two pairs of legs (Min. Alt.-BCB and Min. Alt.-BBL) for water vapor mixing ratio were 1.01 and 1.10 for cloud and clear ensembles, respectively. A similarly calculated ratio for wind speed yielded values of 0.87 (cloud) and 0.83 (clear). The ratio for the turbulence variable σ_{wind} was 1.25 and 1.20 for cloud and clear ensembles,

respectively. When comparing the various forms of N_a differing based on the diameter ranges being examined, the ratio between the two pairs of legs was fairly close to unity for clear and cloud ensembles.

Table 2 summarizes relationship statistics between Min. Alt. and either BCB (cloud ensembles) or BBL (clear ensembles) legs, respectively, including linear best-fit slopes, coefficient of determination (R^2), and MARD. Scatterplots of four selected variables ($N_{a>3nm}$, $N_{a>3270nm}$, θ , water vapor mixing ratio) are shown in Figure 3 (cloud ensembles) and Figure S1 (clear ensembles). The relationships between pairs of legs for the different variables were good (e.g., $R^2 > 0.53$, $MARD \leq 0.44$) for all variables except $N_{a>3270nm}$ (clear and cloud) and H_2O (only clear). Deviating outliers (~ 7 out of 30 points; Figure S1) are linked to special cases of poor mixing in the MBL. Potential temperature exhibited the greatest correlation in MONARC as compared to other variables similar to what will be shown for ACTIVATE subsequently. In cloud ensembles, H_2O exhibited high correlation and similarity between Min. Alt. and BCB legs. For particle number concentration variables, the diameter range of 127–901 nm yielded slightly better results in that slopes were closest to unity (0.93/0.86 for cloud/clear) with high R^2 (0.97/0.83 for cloud/clear) and fairly low MARD (0.26/0.15 for cloud/clear) between pairs of legs. The other size ranges were not too different except for $N_{a>3270nm}$ owing to some points with heightened values in either BCB or BBL as compared to Min. Alt. That the outliers exist in both cloud and clear ensembles suggests that cloud contamination is not the sole possible reason, especially with the use of a strict criteria of $LWC < 0.005 \text{ g m}^{-3}$. A possible contributing factor could be increased humidification at the BCB/BBL levels as compared to the Min. Alt. level leading to increased particle number concentrations with diameters exceeding 3270 nm.

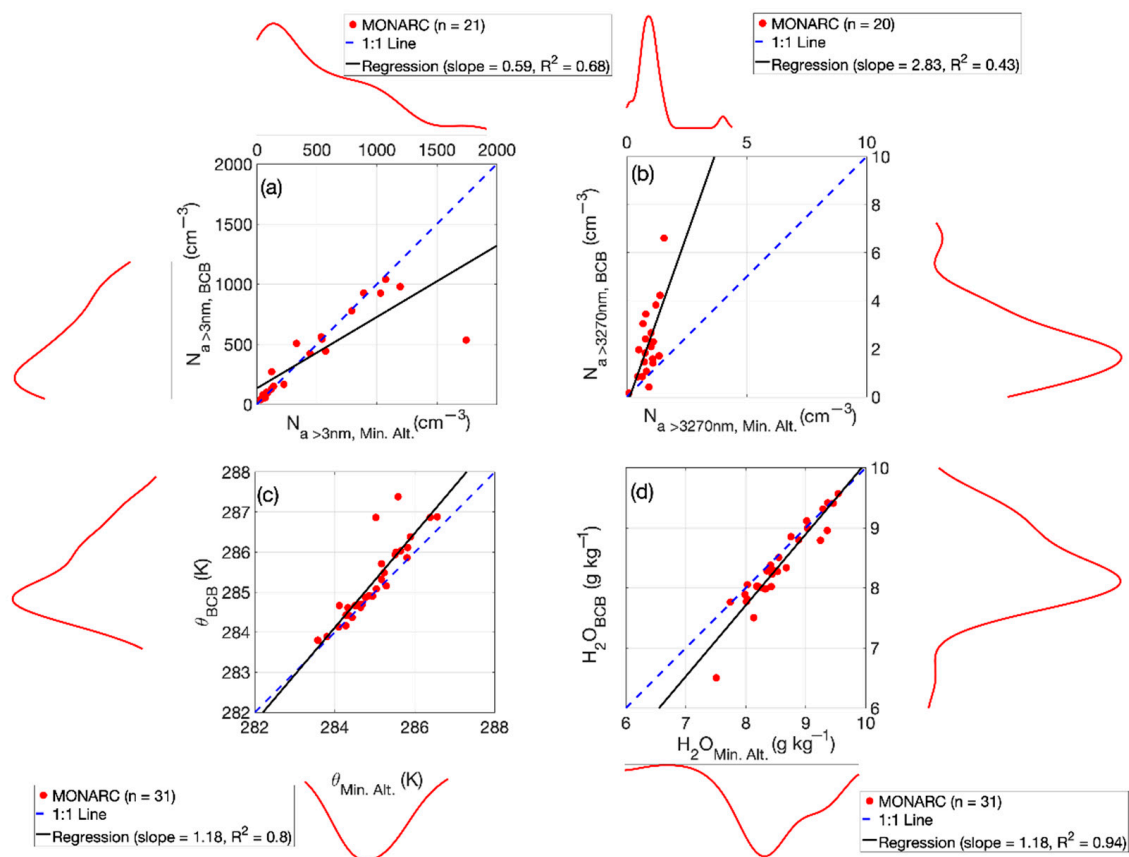


Figure 3. Scatterplots of leg-mean values for selected variables measured in BCB and Min. Alt. legs in cloud ensembles during 2019 MONARC flights. The plots on the sides are marginal distributions based on Kernel density estimation. An analogous figure for clear ensembles in MONARC can be found in Figure S1.

3.1.2. ACTIVATE

The BCB (median ~ 749 m) and BBL (median ~ 613 m) legs were conducted at higher altitudes as compared to the MONARC campaign (Table 3) partly due to the greater variability in MBL structure over the northwest Atlantic as compared to the northeast Pacific [23]. The average horizontal distance between Min. Alt. and BCB (BBL) was 55 (61) km, which was more than twice those from MONARC owing largely to the faster airspeed of the Falcon in ACTIVATE as compared to the Twin Otter in MONARC.

Table 3. Statistics for selected aerosol, gaseous, and meteorological variables measured during ACTIVATE 2020 flights. Statistics are calculated for Min. Alt./BCB legs and Min. Alt./BBL legs for cloud and clear ensembles, respectively, in the first two data columns (additional statistics for 25th/75th percentiles and minimum/maximum values are in Table S2). The rightmost three columns report correlation statistics between different leg pairs conducted at different heights within the MBL for cloud (i.e., Min. Alt. and BCB) and clear (i.e., Min. Alt. and BBL) ensembles, including separation for winter and summer seasons.

Parameter	(Min. Alt./BCB)/(Min. Alt./BBL)		Cloud (All,Summer,Winter)/Clear (All,Summer,Winter)		
	Median	No. Pairs	Slope	R ²	MARD
Altitude (m)	(118/749)/(119/613)	111/54	-	-	-
N _{a>3nm} (cm ⁻³)	(1374/1388)/(3022/2617)	111/54	(0.49,0.89,0.42)/(1.16,1.28,1.13)	(0.63,0.88,0.59)/(0.57,0.61,0.52)	(0.22,0.15,0.27)/(0.36,0.27,0.43)
N _{a>10nm} (cm ⁻³)	(1097/1091)/(2469/2028)	111/54	(0.53,0.89,0.46)/(0.98,1.24,0.91)	(0.67,0.88,0.64)/(0.52,0.62,0.47)	(0.22,0.16,0.27)/(0.34,0.27,0.40)
N _{a100-1000nm} (cm ⁻³)	(247/258)/(520/513)	111/54	(0.90,0.94,0.78)/(0.79,0.81,0.78)	(0.87,0.93,0.70)/(0.76,0.78,0.75)	(0.20,0.15,0.24)/(0.23,0.15,0.29)
N _{a>1000nm} (cm ⁻³)	(0.92/0.85)/(0.63/0.53)	111/54	(0.91,0.86,1.03)/(0.63,0.65,0.52)	(0.81,0.79,0.70)/(0.60,0.60,0.46)	(0.21,0.20,0.22)/(0.42,0.39,0.44)
N _{a>3000nm} (cm ⁻³)	(0.31/0.42)/(0.22/0.14)	106/48	(1.38,1.37,1.66)/(0.96,1.36,0.41)	(0.68,0.75,0.43)/(0.47,0.64,0.14)	(0.36,0.33,0.39)/(0.57,0.46,0.63)
Organic (µg m ⁻³)	(1.01/0.92)/(2.15/2.36)	111/53	(0.95,0.95,0.81)/(0.80,0.69,0.90)	(0.91,0.90,0.78)/(0.84,0.76,0.88)	(0.36,0.40,0.33)/(0.30,0.31,0.29)
Sulfate (µg m ⁻³)	(0.81/0.84)/(0.99/1.02)	111/53	(0.94,0.88,0.90)/(1.00,0.92,0.86)	(0.86,0.83,0.83)/(0.89,0.83,0.77)	(0.20,0.22,0.19)/(0.19,0.16,0.22)
CH ₄ (ppb)	(1968/1969)/(1988/1986)	111/54	(0.95,0.96,0.91)/(0.90,0.98,0.74)	(0.94,0.95,0.87)/(0.82,0.93,0.62)	(0.00,0.00,0.00)/(0.01,0.01,0.01)
CO ₂ (ppm)	(417.7/414.8)/(419.3/418.3)	111/54	(0.97,0.91,0.93)/(0.89,0.75,0.52)	(0.97,0.93,0.88)/(0.83,0.77,0.29)	(0.00,0.00,0.00)/(0.01,0.01,0.01)
CO (ppb)	(129.2/128.9)/(135.3/137.8)	111/54	(0.95,0.97,0.81)/(0.85,1.06,0.63)	(0.95,0.93,0.79)/(0.76,0.92,0.41)	(0.03,0.03,0.02)/(0.06,0.04,0.07)
O ₃ (ppb)	(41.2/41.8)/(45.2/46.0)	110/54	(1.02,1.06,0.95)/(1.00,1.04,0.75)	(0.94,0.92,0.89)/(0.80,0.82,0.66)	(0.04,0.06,0.02)/(0.07,0.10,0.04)
H ₂ O (ppm)	(11422/11351)/(9589/9989)	111/53	(0.99,0.99,0.95)/(0.90,0.87,0.80)	(0.97,0.95,0.92)/(0.93,0.82,0.69)	(0.09,0.06,0.11)/(0.23,0.13,0.31)
wind (m s ⁻¹)	(8.1/7.6)/(6.6/6.4)	109/54	(0.99,0.92,1.03)/(0.82,1.02,0.75)	(0.80,0.80,0.81)/(0.48,0.64,0.43)	(0.18,0.13,0.22)/(0.31,0.21,0.38)
σ _{wind} (m s ⁻¹)	(0.7/0.6)/(0.5/0.3)	111/53	(0.77,0.70,0.78)/(0.54,0.03,0.63)	(0.71,0.79,0.59)/(0.25,0.00,0.32)	(0.24,0.24,0.24)/(0.55,0.58,0.53)
θ (K)	(288.8/289.4)/(286.3/289.9)	111/54	(1.01,1.01,1.03)/(0.99,1.20,1.09)	(0.99,0.98,0.96)/(0.97,0.96,0.88)	(0.00,0.00,0.00)/(0.00,0.00,0.01)

Most variables were similar in value between Min. Alt. and either BCB or BBL legs, consistent with MONARC. Table 3 compares more statistical values when comparing the pairs of legs, including a division between winter and summer seasons to tease out potential differences owing to different meteorological conditions. Potential temperature exhibited the highest correlations most of the time, regardless of cloud/clear conditions or seasons. The slopes (BCB/BBL vs. Min. Alt.) were close to unity except for summer clear ensembles where the slope reached as high as 1.2; Figures 4 and S2 visually show the high degree of correlation between Min. Alt. values and those of either BCB or BBL, respectively. The MARD for potential temperature was generally 0.0 similar to MONARC suggesting that the MBL was usually well mixed.

There were good correlations for gaseous variables including water vapor between pairs of legs ranging from R² = 0.76 for CO in clear ensembles to R² = 0.97 for water vapor and CO₂ in cloud ensembles. Both types of ensembles (clear and cloud) exhibited greater correlations in summer for all gas species. Slopes were close to unity when combining both seasons (0.95–1.02 for cloud and 0.85–1.00 for clear) with clear modules showing more of a difference between seasons with slopes deviating more below unity in the winter. Differences in R² and slope values for winter and summer were highest for CO. This could be linked to the predominant wind direction in winter coming offshore [12,24], resulting in a sharper gradient in anthropogenic pollution as compared to the summer.

For both cloud and clear ensembles, variables related to aerosol number concentration exhibited reduced slopes below unity and a lower level of correlation and similarity between leg pairs as compared to gas measurements. Particles with diameters between 100 and 1000 nm exhibited slopes closest to unity (0.90/0.79 for cloud/clear) with the greatest correlation (R²) and similarity (MARD). The least restrictive size variables (N_{a>3nm} and

$N_{a>10nm}$) had considerably lower slopes in cloud conditions (0.49 and 0.53, respectively) with a significant difference between seasons where they were much closer to unity in summer (0.89 each) in contrast to winter (0.42 and 0.46); a likely explanation could be the higher prevalence of new particle formation events in winter, especially in cloud ensembles, as compared to summer that can yield considerable differences between different vertical levels in the ACTIVATE region [25]. The largest particles ($N_{a>3000nm}$) exhibited slopes of 1.38/0.96 in cloud/clear conditions with correlations similar to the $N_{a>3nm}$ and $N_{a>10nm}$ variables ($R^2 \sim 0.5\text{--}0.7$).

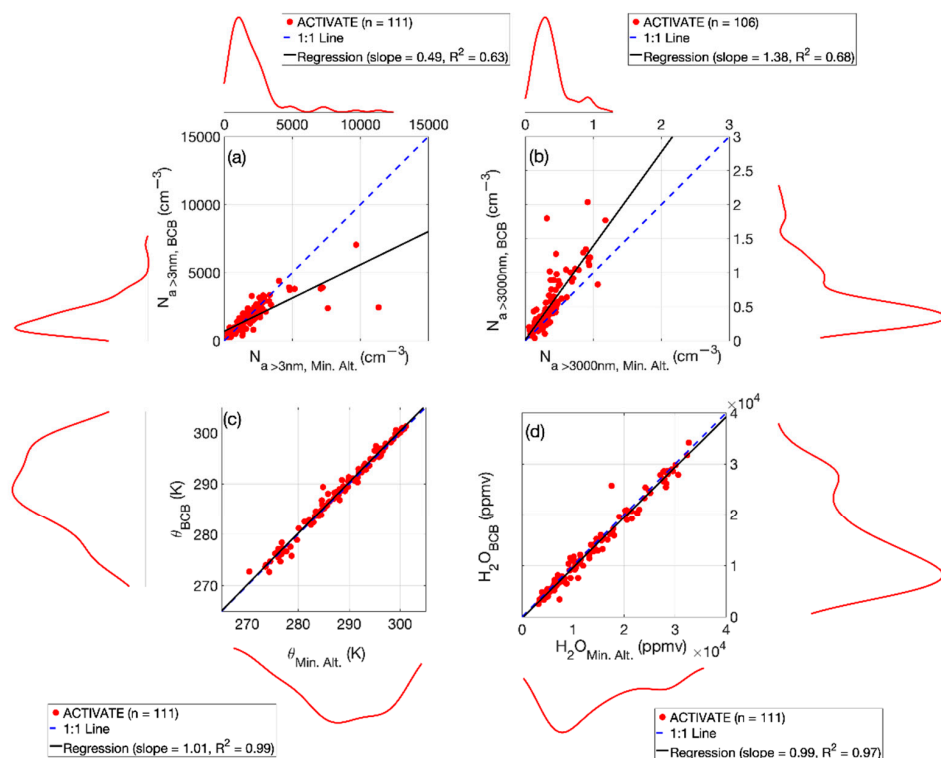


Figure 4. Scatterplots of log-mean values for selected variables measured in BCB and Min. Alt. legs in cloud ensembles during 2020 ACTIVATE flights. The plots on the sides are marginal distributions based on Kernel density estimation. An analogous figure for clear ensembles in ACTIVATE can be found in Figure S2.

Among AMS variables, organic and sulfate consistently exhibited high R^2 (≥ 0.76) and slopes (≥ 0.69) across ensemble types and seasons. Sulfate exhibited the most similarity between pairs of legs between the two seasons and ensemble types, presumably as it exhibits less distinct offshore gradients as compared to organics.

3.2. Horizontal Comparisons

Spatial heterogeneity in data variables for specific leg types (e.g., Min. Alt., BCB) are problematic for data interpretation. Figure 5 demonstrates a case during ACTIVATE research flight 17 on 8 March 2020 where potential temperature exhibits variability both within an individual leg and between legs of the same type throughout a flight. The horizontal gradient in the Min. Alt. leg in Figure 5c would “contaminate” a slant vertical profile conducted around that time, which is evident in Figure 5d. Stairstepping, by design, has the disadvantage that horizontal gradients add uncertainty to the comparison of vertical levels, in the same way that a “wall” flight pattern relies on variables being temporally unchanged across its duration. If horizontal changes are abrupt, such as an air mass gradient, then even adjacent leg comparisons may be ill constrained. In the case of a large-scale gradient, whose characteristic length scale far exceeds the length scale

of the stairstep ensemble, then horizontal and vertical structure may be deconvolved by regridding the observations onto a horizontally coincident location (such as the centroid of an ensemble of stairstep legs).

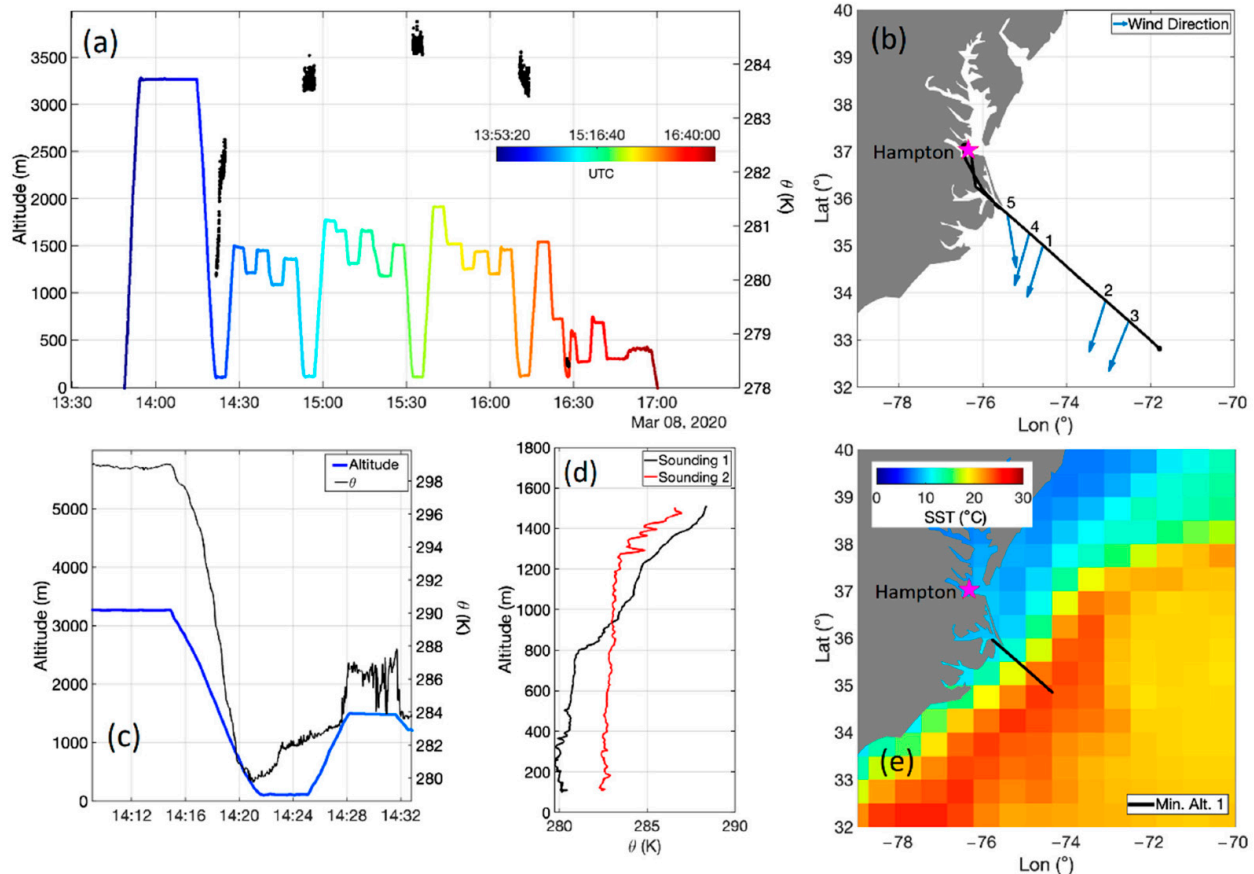


Figure 5. (a) Time series of the HU-25 Falcon altitude (left y-axis; colored by UTC time) and measured potential temperature during Min. Alt. legs (right y-axis; black markers) of research flight 17 on 8 March 2020. (b) Flight tracks for the entire flight with the numbers corresponding to each Min. Alt. leg in order from 1 to 5, with the median wind direction along each of those five legs shown by arrows. (c) Time series of Falcon altitude and potential temperature during a slant descent followed by a Min. Alt. leg (i.e., Min. Alt. 1 in panel (b)) and then an ABL leg during a cloud-free period. (d) Two vertical profiles of potential temperature using data from the slant descent before the first Min. Alt. leg (Sounding 1 in black; UTC 14:18:31–14:21:47) and the slant ascent immediately after that Min. Alt. leg (Sounding 2 in red; UTC 14:25:03–14:28:16). (e) Map showing the location of the first Min. Alt. leg that is examined in more detail in panels c–d. The backdrop is sea surface temperature obtained from the Modern-Era Retrospective Analysis for Research and Applications-Version 2 (MERRA-2) [26] product “inst1_2d_asm_Nx” at 14:00 UTC time, which is closest to the time when the first Min. Alt. leg was conducted.

In the case of Min. Alt. legs (as an example), it would be convenient to use one leg’s worth of data to represent that same altitude in space while an aircraft flies other leg types higher in altitude until the next Min. Alt. leg. If a data user’s application necessitated it, an interpolation technique could be applied to obtain a variable’s value intermediate to two legs of the same type with more success under specific conditions. These conditions include the absence of multiple scales of horizontal variability and/or sharp gradients as compared to no variability or a slowly varying large-scale gradient. To build on these ideas, Table 4 (MONARC) and Table 5 (ACTIVATE) report statistics associated with specific leg types including the slope of variable values along a leg relative to the distance of a leg and

the standard deviation of values along individual legs. Slopes represent the absolute value to remove any dependence on the direction the aircraft flew in.

Table 4. Median values for calculated quantities along individual leg types in MONARC 2019 flights, including the absolute value of the slope of each variable along a leg type (in native units below per km), the “range” (slope multiplied by the distance of a leg type), and the standard deviation. Slopes represent the absolute value to remove any dependence on the direction the aircraft flew in. Standard deviations along single legs were calculated after detrending the data along each leg using linear best fit information as demonstrated in Figure S3.

Parameter	(Min. Alt./BCB)/(Min. Alt./BBL)		
	Slope	Range	Standard Deviation
$N_{a>3nm}$ (cm^{-3})	(2.65/2.53)/(6.14/7.11)	(36/37)/(84/7)	(31/36)/(75/85)
$N_{a>10nm}$ (cm^{-3})	(2.28/2.07)/(4.31/5.60)	(33/29)/(55/6)	(15/17)/(31/20)
$N_{a127-901nm}$ (cm^{-3})	(0.57/0.65)/(0.43/0.44)	(10/9)/(6/0)	(10/10)/(13/13)
$N_{a>901nm}$ (cm^{-3})	(0.0185/0.0258)/(0.0141/0.0184)	(0.25/0.34)/(0.17/0.02)	(1.37/1.35)/(1.53/1.38)
$N_{a>3270nm}$ (cm^{-3})	(0.0181/0.0887)/(0.0055/0.0087)	(0.27/1.19)/(0.08/0.01)	(0.32/0.80)/(0.26/0.26)
H_2O ($g\ kg^{-1}$)	(0.01/0.01)/(0.00/0.01)	(0.1/0.1)/(0.1/0.0)	(0.1/0.1)/(0.1/0.1)
wind ($m\ s^{-1}$)	(0.022/0.038)/(0.051/0.049)	(0.4/0.6)/(0.6/0.0)	(0.6/0.5)/(0.6/0.6)
θ (K)	(0.006/0.008)/(0.006/0.008)	(0.1/0.1)/(0.1/0.0)	(0.1/0.1)/(0.1/0.1)

Table 5. Same as Table 4 but for ACTIVATE 2020 flights.

Parameter	(Min. Alt./BCB)/(Min. Alt./BBL)		
	Slope	Range	Standard Deviation
$N_{a>3nm}$ (cm^{-3})	(4.46/4.89)/(18.11/7.68)	(98/112)/(393/176)	(74/87)/(181/138)
$N_{a>10nm}$ (cm^{-3})	(3.46/3.60)/(13.76/6.30)	(80/83)/(307/160)	(37/52)/(102/97)
$N_{a100-1000nm}$ (cm^{-3})	(1.09/1.07)/(1.02/1.73)	(25/24)/(20/47)	(24/28)/(36/38)
$N_{a>1000nm}$ (cm^{-3})	(0.008/0.0091)/(0.0077/0.0074)	(0.19/0.22)/(0.16/0.17)	(0.97/1.00)/(0.88/0.82)
$N_{a>3000nm}$ (cm^{-3})	(0.0021/0.0043)/(0.002/0.0017)	(0.05/0.10)/(0.04/0.04)	(0.13/0.18)/(0.11/0.10)
Organic ($\mu g\ m^{-3}$)	(0.0119/0.0112)/(0.0159/0.0164)	(0.27/0.25)/(0.31/0.35)	(0.15/0.18)/(0.14/0.18)
Sulfate ($\mu g\ m^{-3}$)	(0.0053/0.0048)/(0.0054/0.0034)	(0.10/0.10)/(0.11/0.08)	(0.05/0.05)/(0.04/0.05)
CH_4 (ppb)	(0.08/0.06)/(0.17/0.16)	(2/2)/(4/4)	(0/1)/(1/2)
CO_2 (ppm)	(0.010/0.010)/(0.021/0.015)	(0.2/0.2)/(0.4/0.3)	(0.1/0.1)/(0.1/0.2)
CO (ppb)	(0.069/0.062)/(0.099/0.100)	(1.6/1.3)/(2.3/2.5)	(3.1/3.2)/(3.2/3.4)
O_3 (ppb)	(0.038/0.029)/(0.059/0.036)	(0.8/0.7)/(1.3/0.7)	(1.0/1.1)/(1.0/1.1)
H_2O (ppm)	(20.22/16.65)/(19.82/34.85)	(453/383)/(395/920)	(261/411)/(256/453)
wind ($m\ s^{-1}$)	(0.023/0.030)/(0.025/0.030)	(0.5/0.7)/(0.6/0.7)	(1.2/0.8)/(1.3/1.3)
θ (K)	(0.009/0.009)/(0.009/0.014)	(0.2/0.2)/(0.2/0.3)	(0.1/0.1)/(0.1/0.1)

Median values of MONARC slopes for a given variable along a leg for an individual leg type are expectedly low relative to typical absolute values of the variables investigated. As an example, potential temperature exhibited a median slope of $\leq 0.008\ K\ km^{-1}$ for the leg types in Table 4, which equates to a total median change of $\leq 0.1\ K$ when accounting for leg distance. The slopes were similar for potential temperature and winds in ACTIVATE but they were somewhat larger for aerosol variables presumably owing to more continental influence leading to stronger offshore gradients as compared to the MONARC region. Similarly, the standard deviation of most aerosol variable values (except supermicrometer N_a variables) were higher for ACTIVATE. Additional statistics associated with the 25th/75th percentile and minimum/maximum values of slopes and standard deviations for MONARC and ACTIVATE can be found in Tables S3–S6 as they can be useful in guiding future types of analyses for these datasets.

Section S1 and Figure S4 report on a different type of horizontal analysis by comparing adjacent BCB legs during ACTIVATE where they were spaced close to one another in each

ensemble. Results point to a high degree of similarity, generally consistent with the other analyses in this section.

One application of the type of results rooted this section is that data users can apply desired threshold values to create an objective “flag” to specify if an ensemble occurred within a homogeneous or slowly varying air mass versus whether it was influenced by rapid changes. This type of flag product can inform data users as to when more or less caution may be warranted when focusing on the horizontal and/or vertical structure of the atmosphere.

4. Case Studies

Case study flight scenarios are now profiled that point to the importance of carefully interpreting field data relying on a stairstepping flight approach. This flight strategy becomes problematic in certain situations highlighted below.

4.1. Sharp Gradients along Level Legs

Sometimes along a level leg there can be considerable variation in values of variables such as potential temperature and water vapor mixing ratio. An example was already shown in Figure 5 where a significant potential temperature gradient was observed during the first Min. Alt. leg of research flight 17 on 8 March 2020. Such a gradient would impact any nearby vertical slant sounding and the ability to apply that leg’s data to adjacent areas less impacted by that small-scale gradient. These types of features were sometimes evident during ACTIVATE by the Gulf Stream edges where significant sea surface temperature gradients impacted the thermodynamic structure of the overlying atmosphere (Figure 5e). Steep gradients within a level leg were most pronounced when winds were aligned along the border of the Gulf Stream (~northerly) rather than being perpendicular (~westerly). In other words, the gradients were steeper when the aircraft was sampling in crosswind conditions, which is the case in Figure 5b with the median wind direction during the first Min. Alt. being 17° (N/NE) in contrast to the aircraft moving southeast (~130°). Figure 5d clearly shows how the two slant profiles on either side of the Min. Alt. leg going over the western border of the Gulf Stream yield a different range of values. Data users are cautioned to subset data near such features to treat them differently. As already noted (e.g., Section 3.1.2), trace gas and aerosol variables can exhibit considerable variability in their concentrations near coastlines of polluted areas with offshore flow.

4.2. Heterogeneous Cloud Base/Top and Boundary Layer Top Heights

Figure 5c highlights a case when a level leg above the MBL top (i.e., ABL leg around UTC 14:28–14:32) goes in and out of the MBL leading to increased variability in variables such as potential temperature. This case has an analogue when the aircraft flies BCB/ACB and BCT/ACT legs since when the aircraft flies level, it can still penetrate in and out of clouds leading to undesired data. Although these issues are not unique to just stairstepping flights (as they also occur for walls), it is important to exercise caution when using data in such scenarios. A simple time series of thermodynamic and cloud variables (e.g., LWC) can reveal when unwanted penetrations are made in or out of either clouds or the MBL.

4.3. Poor Vertical Mixing and Multiple Cloud Layers

4.3.1. MONARC Research Flight 8 (6 June 2019)

MONARC research flight 8 (RF08) on 6 June 2019 is summarized in Figure 6a,b with vertical profiles of potential temperature, LWC, water vapor mixing ratio, and aerosol concentration variables varying in diameter range (>3 nm, 127–901 nm, >3270 nm). Horizontal lines mark the altitudes of various level legs conducted in the ensemble closest to the sounding from which the vertical profiles come from. In this case there were three BBL legs varying in altitude (BBL1 = 510 m, BBL2 = 575 m, BBL3 = 658 m) to better characterize the MBL. This case study is associated with cloud-free conditions.

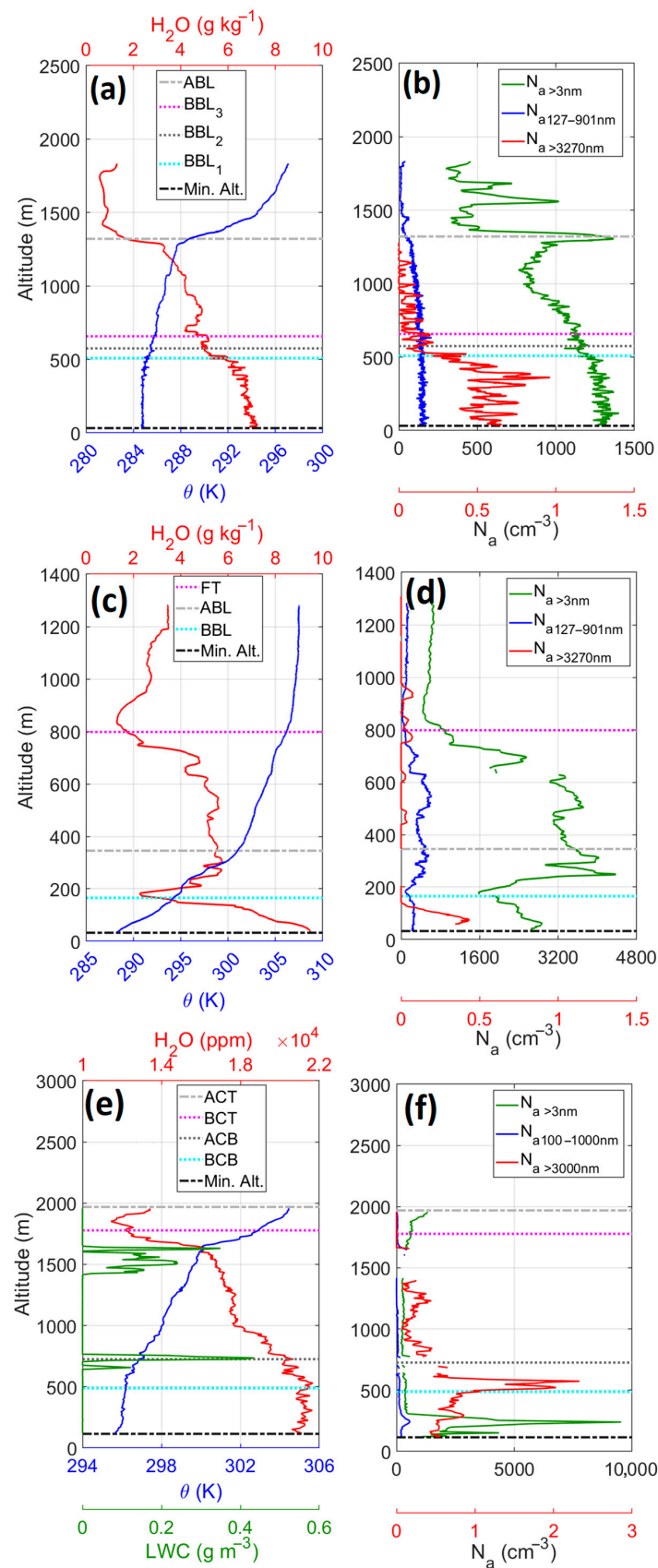


Figure 6. Sounding data for MONARC research flights (RFs) 8 (6 June 2019) and 11 (11 June 2019) and ACTIVATE RF 24 (17 August 2020) in which MBLs were not well mixed. Top (a,b), middle (c,d), and bottom (e,f) are associated with MONARC RF08, MONARC RF11, and ACTIVATE RF24,

respectively. Horizontal lines denote locations of various legs conducted in the closest ensemble to each sounding (see Table 6 for comparative analysis between the legs). MONARC soundings were conducted in clear modules (RF8 = spiral, RF11 = slant) with no cloud layer present whereas the ACTIVATE sounding (slant) was associated with cloud conditions. Sounding times: MONARC RF08 = 6 June 2019, 20:37:52–20:56:58 UTC; MONARC RF11 = 11 June 2019, 19:19:31–19:30:24 UTC; ACTIVATE RF24 = 17 August 2020, 16:30:35–16:34:30 UTC.

Table 6. The differences in leg-mean values for selected variables between Min. Alt. and BBL or BCB for special cases shown in Figure 6. Leg pairs closest in time to the soundings were selected for the comparisons. “–” refers to insufficient data available. For RF08, three BBL legs were conducted and the corresponding numbers are shown in the parentheses in order (left to right) from BBL1 to BBL3.

Parameter	Diff. ^a		
	RF08 (MONARC)	RF11 (MONARC)	RF24 (ACTIVATE)
$N_{a>3nm}$ (cm^{-3})	220,215,287	668	39
$N_{a>10nm}$ (cm^{-3})	188,186,251	432	19
$N_{a\ 127-901nm}$ (cm^{-3}) ^b	40,40,44	74	40
$N_{a>3270nm}$ (cm^{-3}) ^c	0.18,0.22,0.36	–	0.03
H_2O ($g\ kg^{-1}$) ^d	0.9,0.9,2.1	5.9	275
θ (K)	0.3,0.3,1.0	6.0	0.9

^a |Diff. | = $|x_{Min. Alt.} - x_{BCB}|$ or $|x_{Min. Alt.} - x_{BBL}|$. ^b ACTIVATE: $N_{a\ 100-1000nm}$ (cm^{-3}). ^c ACTIVATE: $N_{a>3000nm}$ (cm^{-3}). ^d ACTIVATE: H_2O (ppm).

Potential temperature remained relatively constant (284.8 K–285.0 K) up to 512 m ASL while above that it decreased with altitude until it reached 287.7 K just below the inversion layer base. Water vapor mixing ratio also decreased with altitude but at a slower rate below 512 m as compared to above 512 m. There was a slight decreasing gradient in aerosol concentration up to 512 m with the exception of $N_{a>3270nm}$, which shows fluctuations without a consistent trend up to that altitude. In contrast, above 512 m all three aerosol variables exhibited a sharp drop with altitude, which is likely due to less vertical mixing in the layer decoupled from the surface.

This flight represents a case in which the boundary layer is well mixed up to a certain height in the MBL while the upper portion of the MBL is decoupled from the surface layer. Depending on altitude, there are varying levels of similarity between variables measured in the BBL and Min. Alt. legs. The BBL1 and BBL2 legs closest in altitude to the Min. Alt. leg exhibited decent similarity in aerosol variable values, potential temperature, and water vapor mixing ratio as shown in Table 6; in contrast BBL3 exhibited more deviation with higher potential temperature and reduced values for water vapor mixing and the aerosol concentration variables. For cases such as this in which the MBL is not completely well mixed, stairstepping is a reasonable approach with the caveat that soundings are still critical to include, and that the choice of where to conduct legs and how many to have is critical. For example, a BBL leg closer to 1 km would have very different values compared to even the BBL3 leg. From a data analysis perspective, the sounding data are critical to know how best to intercompare different level legs as the assumption of strong vertical mixing will not always apply.

4.3.2. MONARC Research Flight 11 (11 June 2019)

MONARC RF11 flown on 11 June 2019 was a cloud-free situation similar to RF08. Contrary to RF08, the MBL was detached from near the surface as both potential temperature and water vapor mixing ratio sharply decreased with altitude above the ocean surface. The potential temperature at altitudes relevant to the closest BBL (169 m) and Min. Alt. (36 m) legs were 294.0 and 288.3 K, which is a 1.7 K temperature drop over 133 m. Moreover, the water vapor mixing ratio decreased from 9.5 $g\ kg^{-1}$ (Min. Alt.) to 3.2 $g\ kg^{-1}$ (BBL) equivalent to 6.3 $g\ kg^{-1}$ drop over 133 m demonstrating high stability and very low mixing over the entire MBL.

It is interesting to note that potential temperature continued to decrease with altitude with a similar rate up to 320 m, with a substantial reduction in slope above that point in the free troposphere. On the other hand, the water vapor mixing ratio shows a different trend as it starts to increase just above 169 m and then remains somewhat constant up to 700 m, and above that altitude drops back to lower values. The profile of the water vapor mixing ratio suggests that above the BBL leg altitude there was a different air mass as compared to below.

Up to the altitude at which the BBL leg was conducted (169 m), aerosol concentrations generally dropped except $N_{a>127-901nm}$, which remained relatively constant. Above 169 m, concentrations of $N_{a>3nm}$ and $N_{a>127-901nm}$ increased, and then started to decrease above ~700 m, which resembles the trend for water vapor mixing ratio. $N_{a>3270nm}$ sharply decreased just above the surface which was also evident in RF08 above the decoupled layer, which is likely due to these layers lacking influence of mixing from the ocean surface that is emitting the sea salt particles. The aerosol vertical profiles further confirm the presence of various air masses in the MBL likely because of poor mixing in the MBL. Table 6 further highlights how the differences in variables in MONARC RF11 between Min. Alt. and the BBL leg were large in contrast to RF08.

Overall, RF11 represents a special case of a decoupled boundary layer and sharp gradients in the MBL, representing a scenario in which legs at different altitudes are required to capture the overall picture of MBL. In this case, stairstepping was a decent strategy but the choice of where the legs were placed was very critical and soundings were necessary to fully capture the behavior of the MBL and to inform flight scientists about what level legs to focus on to capture different features. Just like the last case study, data analysis comparing different stairstepping legs for such a case requires extra caution.

4.3.3. ACTIVATE Research Flight 24 (17 August 2020)

Contrary to the previous cases in MONARC, ACTIVATE RF24 on 17 August 2020 was a case study representing a cloudy region, as shown by the LWC profile (Figure 6e). This marine boundary layer consisted of two distinct parts: a bottom layer that is well mixed and coupled to the ocean surface and a top layer that is relatively less mixed. This separation is evident from small changes in potential temperature and water vapor mixing ratio up to 530 m right below a thin cloud layer (~100 m thickness). Above this thin cloud layer, there is a deeper layer characterized by more significant gradients in both potential temperature and water vapor mixing ratio. On top of the second layer there is a deeper cloud layer (215 m), which was a case of a cumulus cloud from below potentially feeding into a larger stratiform cloud deck above.

Aerosol profiles in Figure 6f exhibit interesting characteristics. In the well-mixed bottom layer, $N_{a>3nm}$ and $N_{a100-1000nm}$, contrary to water vapor, exhibit a sharp increase which can be associated with the presence of freshly emitted pollution. This observation highlights the potential for spatial inhomogeneity in aerosol variables owing to strong plumes. This limitation is especially problematic near coastal regions and/or in the presence of freshly emitted particles or new particle formation events when there had not been enough time for mixing in the MBL. $N_{a>3000nm}$ also exhibits an interesting trend, where in the well-mixed bottom layer it increases with altitude with a sharp maximum right below cloud base followed by a downward trend and then another upward trend before reaching the base of the second cloud layer. As with the other two case studies, the stairstepping pattern appeared to provide valuable information but the sounding was critical again as choosing one BCB level is insufficient in cases of multiple cloud layers. A second BCB level would ideally be flown to capture the characteristics below the second deeper layer aloft to link better with cloud legs in that layer.

5. Discussion and Conclusions

Stairstepping is widely used as a flight approach for in situ sampling, especially in campaigns targeting aerosol-cloud interactions. It allows for sampling broader spatial areas

by allowing an aircraft to move forward rather than work in a stacked column such as with a “wall pattern”, while at the same time allowing sufficient time at a level to collect statistics and robust data for instruments with lower time resolution (~minutes). This study presented results focused on examining the variability in atmospheric variable values between level legs as a way of providing context to data users about how best to use data for their applications assuming horizontal and vertical variability impact their intended goals. Most variables investigated exhibited good similarity and correlation between adjacent legs (i.e., Min. Alt. versus BCB/BBL) when the MBL was well mixed. Most similar across the combination of legs compared was potential temperature and trace gases including water vapor mixing ratio. A few variables had reduced similarity such as some aerosol variables (e.g., $N_{a>3nm}$, $N_{a>3000nm}$) for reasons such as spatial inhomogeneity due to coastal gradients or phenomenon such as new particle formation or aerosol humidification. Calculated quantities are provided for both MONARC and ACTIVATE to provide a sense of horizontal variability in a variety of variables in case they can guide decisions about how to interpret data during flights.

Case studies pointed to the importance of not exclusively relying on pre-defined legs such as BCB and BBL in representation of large portions of the MBL owing to the possibility of air masses decoupled from the surface layer and/or when there are multiple cloud levels. Furthermore, level legs penetrating in and out of cloud base/top and MBL top require attention in addition to sharp and short-lived gradients (e.g., along the edge of the Gulf Stream or by polluted coastal areas). For future flight experiments considering stairstepping, the case studies emphasize the importance of the soundings to offer the overall context of the MBL to choose levels carefully to avoid pitfalls such as decoupled layers or multiple cloud layers. Data users should refer to sounding data to understand the MBL structure before relying on the level leg data depending on their specific applications. Issues linked to poor vertical mixing (Sections 4.3.1 and 4.3.2) in this study were shown to often occur in cloud-free conditions since cloudy boundary layers are typically well-mixed. This motivates the use of stairstepping when targeting cloudy conditions.

For some cases such as with deeper MBLs as in ACTIVATE as compared to MONARC, foregoing the Min. Alt. leg for a subset of ensembles in a flight can be favorable if there is a well-mixed MBL. This is because such a strategy saves time and fuel as an aircraft would need to descend a considerable distance below where the cloud layer of interest would be. Furthermore, on a long climb back up to cloud-relevant altitudes, the horizontal gap from the Min. Alt. level to the latter cloud altitudes is higher than a shallower MBL, making it harder to link different parts of a flight if flying in a region prone to sharp gradients. Lastly, owing to the variability in aerosol variables between legs as compared to other studied variables, caution is recommended if trying to use surface-based measurements such as from ships to represent the aerosol impacting clouds.

Supplementary Materials: The following supporting information can be downloaded at: <https://www.mdpi.com/article/10.3390/atmos13081242/s1>. S1. Comparison of Adjacent Below Cloud Base Legs in ACTIVATE. Table S1. Statistics for selected aerosol, gaseous, and meteorological variables measured during the pair of two BCB legs in each cloud ensemble of MONARC 2019 flights. Table S2. Statistics for selected aerosol, gaseous, and meteorological variables measured during adjacent Min. Alt./BCB legs and Min. Alt./BBL legs for cloud and clear ensembles, respectively, for ACTIVATE 2020 flights. Table S3. Statistics for the absolute value of the variable slopes measured during adjacent Min. Alt./BCB legs and Min. Alt./BBL legs for cloud and clear ensembles, respectively, for MONARC 2019 flights. Table S4. Statistics for the standard deviation of variable values measured in cloud and clear legs during MONARC 2019 flights. Table S5. Statistics for the absolute value of the variable slopes measured in cloud and clear legs during ACTIVATE 2020 flights. Table S6. Statistics for the standard deviation of variable values measured in cloud and clear legs during ACTIVATE 2020 flights. Table S7. Statistics for selected aerosol, gaseous, and meteorological variables measured during ACTIVATE 2020 flights. Statistics are calculated for adjacent BCB legs for cloud ensembles in the first two data columns. The rightmost three columns report correlation statistics between the two BCB legs in cloud ensembles, including separation for winter and summer seasons. Figure S1.

Scatterplots of leg-mean values for selected variables measured in BBL and Min. Alt. legs in clear ensembles during 2019 MONARC flights. The plots on the sides are marginal distributions based on Kernel density estimation. Figure S2. Scatterplots of leg-mean values for selected variables measured in BBL and Min. Alt. legs in clear ensembles during 2020 ACTIVATE flights. The plots on the sides are marginal distributions based on Kernel density estimation. Figure S3. Example of removing the linear trend across an individual level leg. (a) Raw data for potential temperature for the Min. Alt. leg in ACTIVATE research flight 4 on 21 February 2020 between UTC 19:14:58 and 19:18:17. (b) Detrended data for the same Min. Alt. leg. Figure S4. Comparison between two consecutive BCB legs for selected variables measured in cloud ensembles during 2020 ACTIVATE flights. Markers represent leg-mean values.

Author Contributions: Conceptualization, H.D., A.S., E.C., M.S. and L.D.Z.; Data curation, E.C., Y.C., A.F.C., J.P.D., G.S.D., S.D., S.K., K.M., R.H.M., J.B.N., C.E.R., M.S., K.L.T., C.V., E.L.W. and L.D.Z.; Formal analysis, H.D. and E.C.; Investigation, H.D., E.C. and A.S.; Methodology, H.D., E.C. and A.S.; Project administration, A.S.; Resources, A.S.; Supervision, A.S.; Writing—original draft, H.D., E.C. and A.S.; Writing—review & editing, Y.C., A.F.C., J.P.D., G.S.D., S.D., S.K., K.M., R.H.M., J.B.N., C.E.R., J.S., M.S., K.L.T., C.V., E.L.W. and L.D.Z. All authors have read and agreed to the published version of the manuscript.

Funding: This research was funded by Office of Naval Research grant N00014-21-1-2115 and NASA grant 80NSSC19K0442 in support of ACTIVATE, a NASA Earth Venture Suborbital-3 (EVS-3) investigation funded by NASA's Earth Science Division and managed through the Earth System Science Pathfinder Program Office. CV and SK thank funding by the DFG CRC 301 TP Change and by HGF W2W3-060.

Institutional Review Board Statement: Not applicable.

Informed Consent Statement: Not applicable.

Data Availability Statement: MONARC Airborne Data: <https://doi.org/10.6084/m9.figshare.5099983.v11> (last accessed 1 July 2022). ACTIVATE Airborne Data: https://doi.org/10.5067/ASDC/ACTIVATE_Aerosol_AircraftInSitu_Falcon_Data_1 (NASA/LARC/SD/ASDC, 2020a) (last accessed 1 July 2022), https://doi.org/10.5067/ASDC/ACTIVATE_Cloud_AircraftInSitu_Falcon_Data_1 (NASA/LARC/SD/ASDC, 2020b) (last accessed 1 July 2022), and https://doi.org/10.5067/ASDC/ACTIVATE_MetNav_AircraftInSitu_Falcon_Data_1 (NASA/LARC/SD/ASDC, 2020c) (last accessed 1 July 2022). MERRA-2 Data: <https://disc.gsfc.nasa.gov/> (last accessed 1 July 2022) [27].

Acknowledgments: The work was funded by both ONR grant N00014-21-1-2115 and NASA grant 80NSSC19K0442 in support of ACTIVATE, a NASA Earth Venture Suborbital-3 (EVS-3) investigation funded by NASA's Earth Science Division and managed through the Earth System Science Pathfinder Program Office. CV and SK thank funding by the DFG CRC 301 TP Change and by HGF W2W3-060.

Conflicts of Interest: The authors declare that they have no conflict of interest.

References

1. Mann, J.; Lenschow, D.H. Errors in airborne flux measurements. *J. Geophys. Res. Atmos.* **1994**, *99*, 14519–14526. [CrossRef]
2. Gerber, H.; Frick, G.; Malinowski, S.P.; Jonsson, H.; Khelif, D.; Krueger, S.K. Entrainment rates and microphysics in POST stratocumulus. *J. Geophys. Res. Atmos.* **2013**, *118*, 12094–12109. [CrossRef]
3. Shingler, T.; Crosbie, E.; Ortega, A.; Shiraiwa, M.; Zuend, A.; Beyersdorf, A.; Ziemba, L.; Anderson, B.; Thornhill, L.; Perring, A.E.; et al. Airborne characterization of subsaturated aerosol hygroscopicity and dry refractive index from the surface to 6.5 km during the SEAC4RS campaign. *J. Geophys. Res. Atmos.* **2016**, *121*, 4188–4210. [CrossRef]
4. Chen, Y.C.; Christensen, M.W.; Xue, L.; Sorooshian, A.; Stephens, G.L.; Rasmussen, R.M.; Seinfeld, J.H. Occurrence of lower cloud albedo in ship tracks. *Atmos. Chem. Phys.* **2012**, *12*, 8223–8235. [CrossRef]
5. Albrecht, B.; Ghate, V.; Mohrmann, J.; Wood, R.; Zuidema, P.; Bretherton, C.; Schwartz, C.; Eloranta, E.; Glienke, S.; Donaher, S.; et al. Cloud System Evolution in the Trades (CSET): Following the Evolution of Boundary Layer Cloud Systems with the NSF–NCAR GV. *Bull. Am. Meteorol. Soc.* **2019**, *100*, 93–121. [CrossRef]
6. McFarquhar, G.M.; Bretherton, C.S.; Marchand, R.; Protat, A.; DeMott, P.J.; Alexander, S.P.; Roberts, G.C.; Twohy, C.H.; Toohy, D.; Siems, S.; et al. Observations of Clouds, Aerosols, Precipitation, and Surface Radiation over the Southern Ocean: An Overview of CAPRICORN, MARCUS, MICRE, and SOCRATES. *Bull. Am. Meteorol. Soc.* **2021**, *102*, E894–E928. [CrossRef]

7. Fast, J.D.; Berg, L.K.; Alexander, L.; Bell, D.; D'Ambro, E.; Hubbe, J.; Kuang, C.; Liu, J.; Long, C.; Matthews, A.; et al. Overview of the HI-SCALE Field Campaign: A New Perspective on Shallow Convective Clouds. *Bull. Am. Meteorol. Soc.* **2019**, *100*, 821–840. [[CrossRef](#)]
8. Schlosser, J.S.; Dadashazar, H.; Edwards, E.L.; Hossein Mardi, A.; Prabhakar, G.; Stahl, C.; Jonsson, H.H.; Sorooshian, A. Relationships Between Supermicrometer Sea Salt Aerosol and Marine Boundary Layer Conditions: Insights from Repeated Identical Flight Patterns. *J. Geophys. Res. Atmos.* **2020**, *125*, e2019JD032346. [[CrossRef](#)]
9. Sorooshian, A.; Anderson, B.; Bauer, S.E.; Braun, R.A.; Cairns, B.; Crosbie, E.; Dadashazar, H.; Diskin, G.; Ferrare, R.; Flagan, R.C.; et al. Aerosol-cloud–Meteorology Interaction Airborne Field Investigations: Using Lessons Learned from the U.S. West Coast in the Design of ACTIVATE off the U.S. East Coast. *Bull. Am. Meteorol. Soc.* **2019**, *100*, 1511–1528. [[CrossRef](#)]
10. Kirschler, S.; Voigt, C.; Anderson, B.; Campos Braga, R.; Chen, G.; Corral, A.F.; Crosbie, E.; Dadashazar, H.; Ferrare, R.A.; Hahn, V.; et al. Seasonal updraft speeds change cloud droplet number concentrations in low-level clouds over the western North Atlantic. *Atmos. Chem. Phys.* **2022**, *22*, 8299–8319. [[CrossRef](#)]
11. Lawson, R.P.; O'Connor, D.; Zmarzly, P.; Weaver, K.; Baker, B.; Mo, Q.; Jonsson, H. The 2D-S (Stereo) Probe: Design and Preliminary Tests of a New Airborne, High-Speed, High-Resolution Particle Imaging Probe. *J. Atmos. Ocean. Technol.* **2006**, *23*, 1462–1477. [[CrossRef](#)]
12. Dadashazar, H.; Painemal, D.; Alipanah, M.; Brunke, M.; Chellappan, S.; Corral, A.F.; Crosbie, E.; Kirschler, S.; Liu, H.; Moore, R.H.; et al. Cloud drop number concentrations over the western North Atlantic Ocean: Seasonal cycle, aerosol interrelationships, and other influential factors. *Atmos. Chem. Phys.* **2021**, *21*, 10499–10526. [[CrossRef](#)] [[PubMed](#)]
13. Moore, R.H.; Thornhill, K.L.; Weinzierl, B.; Sauer, D.; D'Ascoli, E.; Kim, J.; Lichtenstern, M.; Scheibe, M.; Beaton, B.; Beyersdorf, A.J.; et al. Biofuel blending reduces particle emissions from aircraft engines at cruise conditions. *Nature* **2017**, *543*, 411–415. [[CrossRef](#)] [[PubMed](#)]
14. Froyd, K.D.; Murphy, D.M.; Brock, C.A.; Campuzano-Jost, P.; Dibb, J.E.; Jimenez, J.L.; Kupc, A.; Middlebrook, A.M.; Schill, G.P.; Thornhill, K.L.; et al. A new method to quantify mineral dust and other aerosol species from aircraft platforms using single-particle mass spectrometry. *Atmos. Meas. Tech.* **2019**, *12*, 6209–6239. [[CrossRef](#)]
15. Knop, I.; Bansmer, S.E.; Hahn, V.; Voigt, C. Comparison of different droplet measurement techniques in the Braunschweig Icing Wind Tunnel. *Atmos. Meas. Tech.* **2021**, *14*, 1761–1781. [[CrossRef](#)]
16. Sorooshian, A.; MacDonald, A.B.; Dadashazar, H.; Bates, K.H.; Coggon, M.M.; Craven, J.S.; Crosbie, E.; Hersey, S.P.; Hodas, N.; Lin, J.J.; et al. A multi-year data set on aerosol-cloud-precipitation-meteorology interactions for marine stratocumulus clouds. *Sci. Data* **2018**, *5*, 180026. [[CrossRef](#)]
17. DeCarlo, P.F.; Dunlea, E.J.; Kimmel, J.R.; Aiken, A.C.; Sueper, D.; Crouse, J.; Wennberg, P.O.; Emmons, L.; Shinozuka, Y.; Clarke, A.; et al. Fast airborne aerosol size and chemistry measurements above Mexico City and Central Mexico during the MILAGRO campaign. *Atmos. Chem. Phys.* **2008**, *8*, 4027–4048. [[CrossRef](#)]
18. Gerber, H.; Arends, B.G.; Ackerman, A.S. New microphysics sensor for aircraft use. *Atmos. Res.* **1994**, *31*, 235–252. [[CrossRef](#)]
19. DiGangi, J.P.; Choi, Y.; Nowak, J.B.; Halliday, H.S.; Diskin, G.S.; Feng, S.; Barkley, Z.R.; Lauvaux, T.; Pal, S.; Davis, K.J.; et al. Seasonal Variability in Local Carbon Dioxide Biomass Burning Sources Over Central and Eastern US Using Airborne in Situ Enhancement Ratios. *J. Geophys. Res. Atmos.* **2021**, *126*, e2020JD034525. [[CrossRef](#)]
20. Diskin, G.; Podolske, J.; Sachse, G.; Slate, T. *Open-Path Airborne Tunable Diode Laser Hygrometer*; SPIE: Bellingham, WA, USA, 2002; Volume 4817.
21. Thornhill, K.L.; Anderson, B.E.; Barrick, J.D.W.; Bagwell, D.R.; Friesen, R.; Lenschow, D.H. Air motion intercomparison flights during Transport and Chemical Evolution in the Pacific (TRACE-P)/ACE-ASIA. *J. Geophys. Res. Atmos.* **2003**, *108*. [[CrossRef](#)]
22. Sinnott, R.W. Virtues of the Haversine. In *Sky and Telescope*; Sky Publishing Corporation: Lincolnshire, IL, USA, 1984; Volume 68, p. 159.
23. Gonzalez, M.E.; Corral, A.F.; Crosbie, E.; Dadashazar, H.; Diskin, G.S.; Edwards, E.-L.; Kirschler, S.; Moore, R.H.; Robinson, C.E.; Schlosser, J.S.; et al. Relationships between supermicrometer particle concentrations and cloud water sea salt and dust concentrations: Analysis of MONARC and ACTIVATE data. *Environ. Sci. Atmos.* **2022**, *2*, 738–752. [[CrossRef](#)]
24. Painemal, D.; Corral, A.F.; Sorooshian, A.; Brunke, M.A.; Chellappan, S.; Afzali Gorooh, V.; Ham, S.-H.; O'Neill, L.; Smith, W.L., Jr.; Tselioudis, G.; et al. An Overview of Atmospheric Features Over the Western North Atlantic Ocean and North American East Coast—Part 2: Circulation, Boundary Layer, and Clouds. *J. Geophys. Res. Atmos.* **2021**, *126*, e2020JD033423. [[CrossRef](#)]
25. Corral, A.F.; Choi, Y.; Crosbie, E.; Dadashazar, H.; DiGangi, J.P.; Diskin, G.S.; Fenn, M.; Harper, D.B.; Kirschler, S.; Liu, H.; et al. Cold Air Outbreaks Promote New Particle Formation Off the U.S. East Coast. *Geophys. Res. Lett.* **2022**, *49*, e2021GL096073. [[CrossRef](#)]
26. Gelaro, R.; McCarty, W.; Suárez, M.J.; Todling, R.; Molod, A.; Takacs, L.; Randles, C.; Darmenov, A.; Bosilovich, M.G.; Reichle, R.; et al. The Modern-Era Retrospective Analysis for Research and Applications, Version 2 (MERRA-2). *J. Clim.* **2017**, *30*, 5419–5454. [[CrossRef](#)]
27. Global Modeling and Assimilation Office (GMAO). Goddard Earth Sciences Data and Information Services Center (GES DISC). Available online: <https://disc.gsfc.nasa.gov/> (accessed on 1 June 2022).